

Simulation of a Pion Photodetection Experiment

by

Angel Roberto Solis Ortíz

Submitted to the Department of Physics
in partial fulfillment of the requirements for the degree of
Bachelor of Science in Physics

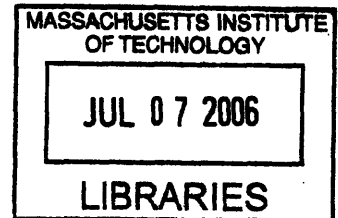
at the

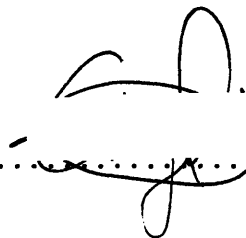
MASSACHUSETTS INSTITUTE OF TECHNOLOGY

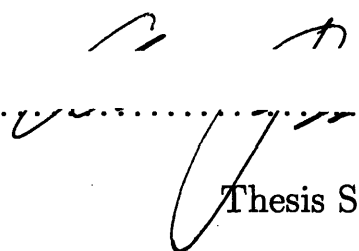
June 2006

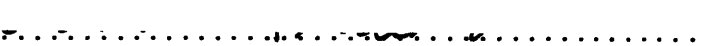
© Angel Roberto Solis Ortíz, MMVI. All rights reserved.

The author hereby grants to MIT permission to reproduce and
distribute publicly paper and electronic copies of this thesis document
in whole or in part.



Author  **ARCHIVES**
Department of Physics
May 12, 2006

Certified by 
Professor Aron M. Bernstein
Thesis Supervisor, Department of Physics

Accepted by 
Professor David E. Pritchard
Senior Thesis Coordinator, Department of Physics

Simulation of a Pion Photodetection Experiment

by

Angel Roberto Solis Ortiz

Submitted to the Department of Physics
on May 12, 2006, in partial fulfillment of the
requirements for the degree of
Bachelor of Science in Physics

Abstract

In this thesis we assess the capabilities of the Crystal Box detector and evaluate its advantages over the Neutral Meson Spectrometer (NMS) detector in a planned experiment at the High Intensity Gamma Source (HI γ S) at Duke University. After discussing the relevance of the experiment and briefly reviewing the physics at play, we delve into the details of the Crystal Box detector and explain how it is being modeled in the simulation. We calculate the acceptance of each detector and their resolution in measuring physical quantities from each pion photoproduction event detected. We then simulate the extraction of raw data from the experiment using both the Crystal Box and the NMS detectors, and present our results as to how well we believe each detector will perform at measuring the physical quantities of interest. Finally, we discuss possible refinements that could be implemented in the simulation to further improve the accuracy of these predictions.

Thesis Supervisor: Professor Aron M. Bernstein

Acknowledgments

I would like to express my sincere gratitude to Professor Aron M. Bernstein for giving the opportunity of working under his supervision, and for his patient guidance which made my thesis work possible.

This thesis marks the culmination of my undergraduate education and it would have been impossible without the people that supported me throughout my years at MIT. My dearest thanks go to Sarah Gonzalez whose patience and unconditional support helped me get through many sleepless nights and endless piles of work without losing my sanity. I would also like to thank my father Israel Solis and my grandparents Sofia Jimenez and Miguel Angel Solis for teaching me the most valuable skills I have through their wise guidance, discipline, and endless love.

Last I would like to dedicate this work to both my grandfather Dr. Roberto Ortiz and my great-grandfather Félix Ortiz. *A pesar de su partida, el ejemplo de sus vidas ha sido mi mayor inspiración durante todos estos años.*

Contents

1	Introduction	7
2	The Experiment	9
2.1	Pion photoproduction	9
2.2	Experimental setup	12
2.3	The Crystal Box	13
2.4	The NMS detector	15
3	Implementation of the Simulation	16
3.1	Geometry of the Crystal Box	16
3.2	Organization of tasks	19
4	Results from the Simulation	21
4.1	Properties of the detectors	21
4.2	Fits to the simulation data	28
5	Conclusions	37
5.1	Performance of the detectors	37
5.2	Limitations of the simulation	37

List of Figures

2-1	Diagram illustrating the design of the Crystal Box	13
2-2	Diagram illustrating the design of the NMS detector	15
3-1	Coordinate system on each face of the Crystal Box	17
4-1	Mean acceptance as a function of the target shift	22
4-2	Acceptances of NMS and Crystal Box detectors	22
4-3	Slices of the acceptance of the NMS detector	23
4-4	Slices of the acceptance of the Crystal Box	24
4-5	Different resolutions of the NMS detector	26
4-6	Different resolutions of the Crystal Box	27
4-7	Fits to simulated cross section data (1)	30
4-8	Fits to simulated cross section data (2)	31
4-9	Fits to simulated cross section data (3)	32
4-10	Fits to simulated cross section data (4)	33
4-11	Fits to simulated cross section data (5)	34
4-12	Fits to simulated cross section data (6)	35
4-13	Fits to simulated cross section data (7)	36

List of Tables

3.1	Numbering of the faces of the Crystal Box	17
3.2	Distribution of fundamental sources of error	18
3.3	Script names and description of their tasks	20
4.1	Acceptances and resolutions of both detectors	25
4.2	Fits to simulation data using NMS detector	28
4.3	Fits to simulation data using Crystal Box	29

Chapter 1

Introduction

Chiral perturbation theory (ChPT) is an effective-field theory built on a Lagrangian that exhibits chiral symmetry on the limit where the light quark masses m_u and m_d are set to zero (the chiral limit). The theory provides a useful low-energy representation of QCD [1]. Since pions are considered the pseudo Nambu-Goldstone bosons of spontaneously broken chiral symmetry, ChPT allows the description of interactions between pions, and between pions and nucleons [2]. Calculations of the amplitude for threshold pion photoproduction are in impressive agreement with experiments carried out at Mainz [3] and Saskatoon. In addition, an experiment at Brookhaven has found the low-energy $\pi\pi$ phase shifts to be in agreement with ChPT calculations [2].

The success of low-energy πN scattering and pion photo- and electroproduction experiments demonstrates that the pion is the pseudo Nambu-Goldstone boson of QCD and that its low-energy production and interactions vanish in the chiral limit. Despite these successes, not all of the chiral predictions have been verified yet. None of the experiments completed to date are accurate enough to test the isospin-breaking predictions of low energy $\pi^0 N$ scattering. The relatively large value of the isospin-breaking quantity relevant in $\pi^0 N$ scattering, $\frac{m_d - m_u}{m_d + m_u} \simeq 30\%$, presents an unusual experimental opportunity to test the consequences of $m_d - m_u > 0$ through the use of the pion photoproduction reaction with polarized targets [2].

The main purpose of this thesis is to assess the capabilities of the Crystal Box detector in a planned experiment at the High Intensity Gamma Source (HI γ S) facility

at Duke University which is expected to make accurate measurements of double polarization (both beam and target) observables. These measurements will rigorously test ChPT calculations and predictions of isospin breaking due to $m_d - m_u > 0$. The original setup for such experiment incorporated the Neutral Meson Spectrometer (NMS) detector whose capabilities were evaluated in an undergraduate thesis by Ethan Howe [4]. Since then, the experimenters have decided to switch to the use of the Crystal Box detector whose much larger solid angle coverage is expected to significantly improve the statistics of the planned experiment, thus helping them make more precise measurements of the double-polarization observables.

In order to evaluate the capabilities of the Crystal Box detector, we will simulate the production and detection of pions from the reaction $\vec{\gamma}\vec{p} \rightarrow \pi^0 p$ using full initial state polarizations while taking into account the dominant sources of error in the experiment. Calculating the resolution with which we measure the pion cross section will enable us to obtain a reasonable estimate of the resolution at which we can measure the pion multipole amplitudes, and we will use this to compare the advantages of choosing the Crystal Box over the NMS detector. We will also discuss possible refinements that could be implemented in the simulation to further improve the accuracy of these predictions.

Chapter 2

The Experiment

2.1 Pion photoproduction

The planned experiment at HI γ S aims at observing the production of pions from the reaction $\vec{\gamma}\vec{p} \rightarrow \pi^0 p$ by striking a proton-rich polarized target with a beam of linearly- and circularly-polarized photons. The cross section for the pions generated by this reaction is:

$$\begin{aligned} \frac{d\sigma}{d\Omega} = \frac{p_\pi^*}{k_\gamma^*} \{ & R_T^{00} + P_T {}^c R_{TT}^{00} \cos 2\varphi + P_x (P_\odot R_{TT'}^{0x} - P_T {}^s R_{TT}^{0x} \sin 2\varphi) \\ & + P_y (R_T^{0y} + P_T {}^c R_{TT}^{0y} \cos 2\varphi) + P_z (P_\odot R_{TT'}^{0z} - P_T {}^s R_{TT}^{0z} \sin 2\varphi) \} \end{aligned} \quad (2.1)$$

where p_π^* and k_γ^* are the pion and photon center-of-mass momenta respectively, φ is the angle between the polarization vector of the photon and the reaction plane, P_T and P_\odot are the degrees of linear and circular polarization of the photon, and $P_{x,y,z}$ are the degrees of target polarization in the coordinate basis of the lab [4, 5].

The cross section described in equation 2.1 is composed from a set of eight structure functions $R_i^{\beta\alpha}$ which, being the bilinear products of the electromagnetic transition matrix elements, encode information about photopion dynamics. At the present time and in the threshold region, all existing measurements are of the unpolarized structure function R_T , and there is only one measurement at a specific energy of the polarized-photon observable ${}^c R_{TT}^{00}$ [3]. A measurement of the polarized-target observable R_T^{0y} is

of tremendous importance since it contains effects due to isospin breaking. This measurement would test two independent claims of isospin violation in medium-energy πN scattering to a degree that is in substantial disagreement with ChPT calculations [6, 7]. The five remaining structure functions ${}^cR_{TT}^{0y}$, $R_{TT'}^{0x}$, $R_{TT'}^{0z}$, ${}^sR_{TT}^{0x}$ and ${}^sR_{TT}^{0z}$ are double-polarization observables requiring both polarized beams and targets. These structure functions have never been measured and some are required to perform a model-independent determination of the multipole amplitudes [2].

There are many competing theoretical models that predict these observables in the near-threshold region including ChPT one-loop, MAID [8], and DMT [9, 10] model calculations, but the only existing measurement of ${}^cR_{TT}^{00}$ is in disagreement with the DMT prediction [9, 10]. The proposed experiment at HI γ S would help by either verifying or dismissing this discrepancy and stringently testing other predictions made by these theoretical and model calculations.

The response functions $R_i^{\beta\alpha}$ are real or imaginary parts of bilinear forms of the Chew, Goldberger, Low and Nambu (CGLN) amplitudes F_i [5]:

$$R_T^{00} = \Re[(F_2^* F_3 + F_1^* F_4 + F_3^* F_4 \cos \theta^*) \sin^2 \theta^* - 2F_1^* F_2 \cos \theta^*] + |F_1|^2 + |F_2|^2 + \frac{1}{2}(|F_3|^2 + |F_4|^2) \sin^2 \theta^* \quad (2.2a)$$

$$R_T^{0y} = \Im[F_1^* F_3 - F_2^* F_4 + (F_1^* F_4 - F_2^* F_3) \cos \theta^* - F_3^* F_4 \sin^2 \theta^*] \sin \theta^* \quad (2.2b)$$

$${}^cR_{TT}^{00} = \Re[F_2^* F_3 + F_1^* F_4 + F_3^* F_4 \cos \theta^*] \sin^2 \theta^* + \frac{1}{2}(|F_3|^2 + |F_4|^2) \sin^2 \theta^* \quad (2.2c)$$

$${}^sR_{TT}^{0x} = \Im[2F_1^* F_2 + F_1^* F_3 - F_2^* F_4 + (F_1^* F_4 - F_2^* F_3) \cos \theta^*] \sin \theta^* \quad (2.2d)$$

$${}^cR_{TT}^{0y} = \Im[2F_1^* F_2 + F_1^* F_3 - F_2^* F_4 - F_3^* F_4 \sin^2 \theta^* + (F_1^* F_4 - F_2^* F_3) \cos \theta^*] \sin \theta^* \quad (2.2e)$$

$${}^sR_{TT}^{0z} = \Im[-F_2^* F_3 - F_1^* F_4] \sin^2 \theta^* \quad (2.2f)$$

$$R_{TT'}^{0x} = \Re[F_1^* F_3 - F_2^* F_4 + (F_1^* F_4 - F_2^* F_3) \cos \theta^*] \sin \theta^* \quad (2.2g)$$

$$R_{TT'}^{0z} = \Re[2F_1^* F_2 \cos \theta^* - (F_1^* F_4 + F_2^* F_3) \sin^2 \theta^*] - |F_1|^2 - |F_2|^2 \quad (2.2h)$$

Furthermore, the CGLN amplitudes F_i are functions of the center of mass scattering angle θ^* and the multipoles $E_{l\pm}$, $M_{l\pm}$ and $L_{l\pm}$ characterizing the electric (E), magnetic

(M) and longitudinal (L) excitation mechanisms. The explicit connection between the relevant CGLN amplitudes and the multipoles is given by a sum over all values of the total angular momentum l in terms of the Legendre polynomials $P_l(\cos\theta^*)$ [5]:

$$F_1 = \sum_{l \geq 0} [(E_{l+} + M_{l+}) P'_{l+1} + (E_{l-} + (l+1)M_{l-}) P'_{l-1}] \quad (2.3a)$$

$$F_2 = \sum_{l \geq 1} [(l+1) M_{l+} + l M_{l-}] P'_l \quad (2.3b)$$

$$F_3 = \sum_{l \geq 1} [(E_{l+} - M_{l+}) P''_{l+1} + (E_{l-} + M_{l-}) P''_{l-1}] \quad (2.3c)$$

$$F_4 = \sum_{l \geq 2} [M_{l+} - E_{l+} - M_{l-} - E_{l-}] P''_l \quad (2.3d)$$

Near threshold one can simplify these expressions by assuming that pions are produced only with angular momentum l_π of zero and one. Because of parity and angular momentum conservation only the s -wave amplitude E_{0+} ($l_\pi = 0$) and the p -wave amplitudes $M_{1\pm}$ and E_{1+} ($l_\pi = 1$) can contribute. This approximation leads to a great deal of computational simplification. For example, the equations for the unpolarized and single-polarization observables reduce to [3]:

$$R_T^{00} = 2\Re[E_{0+}^* (3E_{1+} - M_{1+} + M_{1-})] \cos\theta^* + |3E_{1+} - M_{1+} + M_{1-}|^2 \cos^2\theta^* \\ + |E_{0+}|^2 + \frac{1}{2} (|2M_{1+} + M_{1-}|^2 + |3E_{1+} - M_{1+} + M_{1-}|^2) \sin^2\theta^* \quad (2.4a)$$

$$R_T^{0y} = 3\Im[E_{0+}^* (E_{1+} - M_{1+}) - (E_{1+}^* (4M_{1+} - M_{1-}) + M_{1+}^* M_{1-}) \cos\theta^*] \sin\theta^* \quad (2.4b)$$

$${}^cR_{TT}^{00} = \left(\frac{9}{2} |E_{1+}|^2 - \frac{3}{2} |M_{1+}|^2 - 3\Re[E_{1+}^* (M_{1+} - M_{1-}) + M_{1+}^* M_{1-}]\right) \sin^2\theta^* \quad (2.4c)$$

Each of the multipoles is a complex number, but one can take advantage of the fact that the p -wave phase shifts are small in the threshold region and make the additional assumption that all p -wave related multipoles are purely real. Hence, by measuring all the response functions through the full beam and target polarization cross section described in equation 2.1, one can simultaneously measure both real and

imaginary parts of E_{0+} , and the real parts of the E_{1+} , M_{1-} and M_{1+} multipoles by fitting the functional form of the cross section to only these five parameters. All of these approximations are easy to lift. Given an accurate measurement of the response functions (and hence of the CGLN amplitudes), we can invert equations 2.3 and take advantage of the orthonormality of Legendre polynomials to obtain expressions for *all* multipoles $E_{l\pm}$, $M_{l\pm}$ and $L_{l\pm}$ in terms of integrals of the CGLN amplitudes over θ^* [5]. However we want to keep our simulation computationally inexpensive and as a result we shall test our simulation using only the s - and p -wave approximations.

2.2 Experimental setup

The anticipated experiment at the HI γ S facility is expected to use a fully polarized photon beam of intensity $I \simeq 6 \times 10^6$ photons/sec. The energies of individual photons follow a distribution that is narrowly centered at 158 MeV with a spread of 2% fwhm. The photon beam is aimed at a polarized plastic scintillator target measuring 10 cm in length with an areal density of $N_T \simeq 2 \times 10^{23}$ protons/cm². A tiny fraction of these photons will interact with the polarized protons in the target through the $\vec{\gamma}\vec{p} \rightarrow \pi^0 p$ reaction. The use of a plastic scintillator allows us to exclude the pions produced from the heavy elements in the target (primarily ¹²C) by screening out events with very low recoil energies [2]. Given these parameters, we expect to produce neutral pions at the rate of $I \cdot N_T \cdot \sigma_{TOT} \simeq 7 \times 10^3$ pions/hour.

The pions produced in this reaction will be ejected in directions distributed according to the cross section described in equation 2.1. The resulting pions have a mean life less than 10^{-16} sec and thus they may be regarded as instantly decaying through their main decay mode $\pi^0 \rightarrow \gamma\gamma$. In the rest frame of the pion both γ -rays are produced back to back and with no preferred direction. We will be able to reconstruct the momentum of the π^0 if and only if we are able to measure the momenta of both γ -rays using our detector. Finally, we will measure the cross section of the given reaction by observing the angular distribution of many π^0 production events.

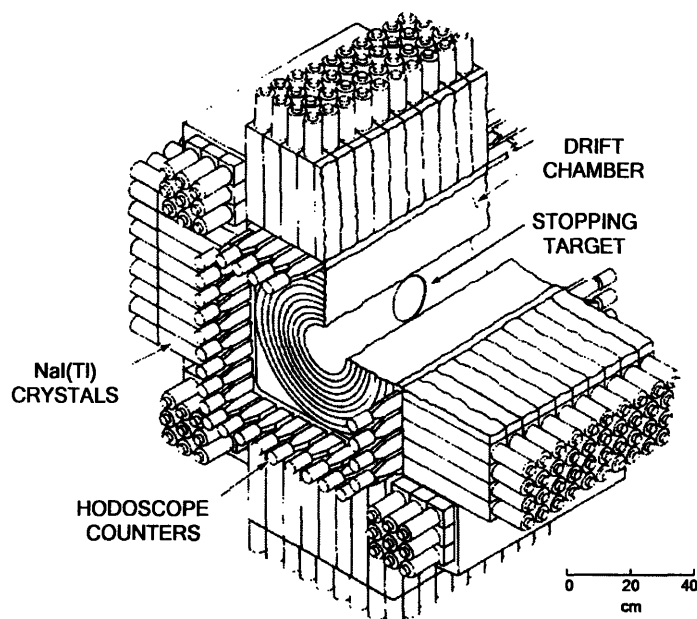


Figure 2-1: Diagram of the Crystal Box detector [11]. We will only use crystals in the largest four arrays and will disregard the 3×3 crystal arrays located at the corners.

2.3 The Crystal Box

The detector to be used in the planned experiment is the Crystal Box. This detector is built using 396 highly polished NaI(Tl) crystal modules. It provides both a large solid angle of coverage and good resolution for impact location, and time of impact and γ -ray energy. The first 360 crystals have dimensions of $2.5'' \times 2.5'' \times 12''$ and are arranged into four 10×9 arrays in transverse orientation with respect to each other as depicted in figure 2-1. The remaining 36 crystals have dimensions of $2.5'' \times 2.5'' \times 30''$ and are arranged in 3×3 arrays located at the corners, but there are no current plans to use these in the experiment.

When a γ -ray deposits itself into a particular crystal, a somewhat small fraction of its energy leaks over to adjacent crystals. The energy in each crystal is then picked up by a photomultiplier tube (PMT) attached to the crystal and converted into a linear output current which is registered by an array of electronics. A detailed discussion of the NaI(Tl) signal chain is provided by S.L Wilson et al. [11] but we shall find it sufficient to know that our array of electronics will record energy deposited in every

crystal after going through a calibration procedure. Measurement of an incoming γ -ray's energy is achieved by finding the crystal module with the highest energy and summing the energies deposited in neighboring crystals. The detected energy for a given γ -ray will fluctuate with the point of impact because the pattern of energy leakage will vary depending on the point of entry within the crystal and the position of the entry crystal relative to the array. This effect and the intrinsic resolution of each crystal-PMT detector combine into a γ -ray energy resolution which varies very slowly from 8% fwhm at 55 MeV to 7% fwhm at 129.4 MeV. The energy resolution of the Crystal Box is somewhat inferior than that of the NMS detector, which provides resolutions of 5% fwhm and 4% fwhm at the same γ -ray energies, respectively [11]. For our purpose we can safely assume the energy resolution of the Crystal Box is a constant 8% fwhm.

The point \mathbf{x} where a γ -ray impacts one of the faces of the Crystal Box is estimated as the weighted centroid of the deposited energy distribution according to the equation $\mathbf{x} = \sum \mathbf{x}_i E_i^\beta / \sum E_i^\beta$, where the index i summed over all of the array's modules with energy greater than 0.5 MeV. Wilson et al. found that the value $\beta = 0.55$ is optimal for detecting γ -rays by analyzing Monte Carlo events and minimizing the resolution with which the reconstructed position can be determined [11]. This procedure leads to difficulties when attempting to calculate the position of any γ -ray that lands on an outer edge crystal since the energy leakage patterns are significantly different from those of inner crystals. The current plan is therefore to ignore the detection of any γ -ray that lands on any of the outer edge crystals. The hit position resolution found for the Crystal Box is 1.9 cm (fwhm) averaged over the area of a crystal array, which is also inferior to the average resolution of 1.5 cm (fwhm) that the NMS detector offers. Despite having slightly inferior position and energy resolutions, we still expect the Crystal Box detector to perform better than the NMS detector in our experiment because (as we shall see in Chapter 4) its mean acceptance (the fraction of pion production events that are actually detected) is about an order of magnitude larger than the mean acceptance of the NMS detector.

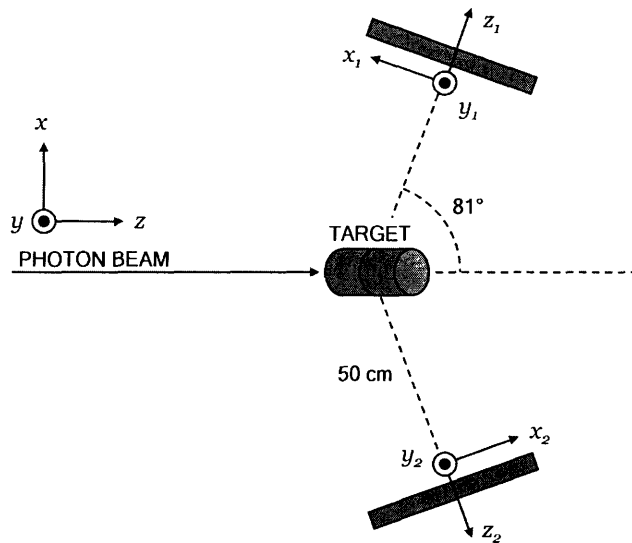


Figure 2-2: Diagram of the NMS detector. The coordinates for detector faces 1 and 2 are defined relative to the lab's coordinates. The y -direction is normal to the floor.

2.4 The NMS detector

The Neutral Meson Spectrometer (NMS) was built at Los Alamos Meson Physics Facility. Each of the two detector faces consists of a 4×8 array of CsI crystals placed at an angle of 81 degrees from the direction of the beam at a distance of 50 cm (see figure 2-2). Each array of crystals has dimensions of $2.5 \text{ cm} \times 2.5 \text{ cm}$ (x_i versus y_i).

The NMS was the original detector with which the experiment was planned, and its capabilities were evaluated in an undergraduate thesis by Ethan Howe [4]; since then, the experimenters have opted to use the Crystal Box detector instead. Given our desire to evaluate the advantages offered by the Crystal Box, we decided to base our simulation on the same framework used by Howe's simulation of the NMS detector while making many improvements, such as adding support for multiple target and photon polarizations, and implementing the geometry of the Crystal Box detector. We shall not delve deeper into any more details of the NMS detector, but we will frequently draw back to back comparisons between the results of our simulation using the Crystal Box and the NMS detectors.

Chapter 3

Implementation of the Simulation

3.1 Geometry of the Crystal Box

Implementing the geometry of the Crystal Box detector into our simulation involves three major steps. First, we need to figure out if and where each of the γ -rays hits any of the faces of the detector. For the Crystal Box, we find it convenient to define a coordinate system on each of the faces of the detector such that the coordinates rotate into each other if the detector were rotated by 90° about the axis of the photon beam as illustrated in figure 3-1. We also assign a number n to each face in order of increasing ϕ . After Lorentz-transforming the momentum of each γ -ray from the center of mass frame into the lab frame and calculating the angles θ and ϕ that describe its direction in the lab frame, we use the conditions in table 3.1 to determine which face a γ -ray would hit if it were to land on the detector as a function of ϕ . We proceed by assigning coordinates to the impact point where the γ -ray *actually* hits the detector face. Referring to figure 3-1 and using a little trigonometry, it is not hard to show that these coordinates are given by:

$$x_{actual} = w \tan(\phi - n\pi/2) \tag{3.1a}$$

$$y_{actual} = w \sec(\phi - n\pi/2) \cot \theta - s \tag{3.1b}$$

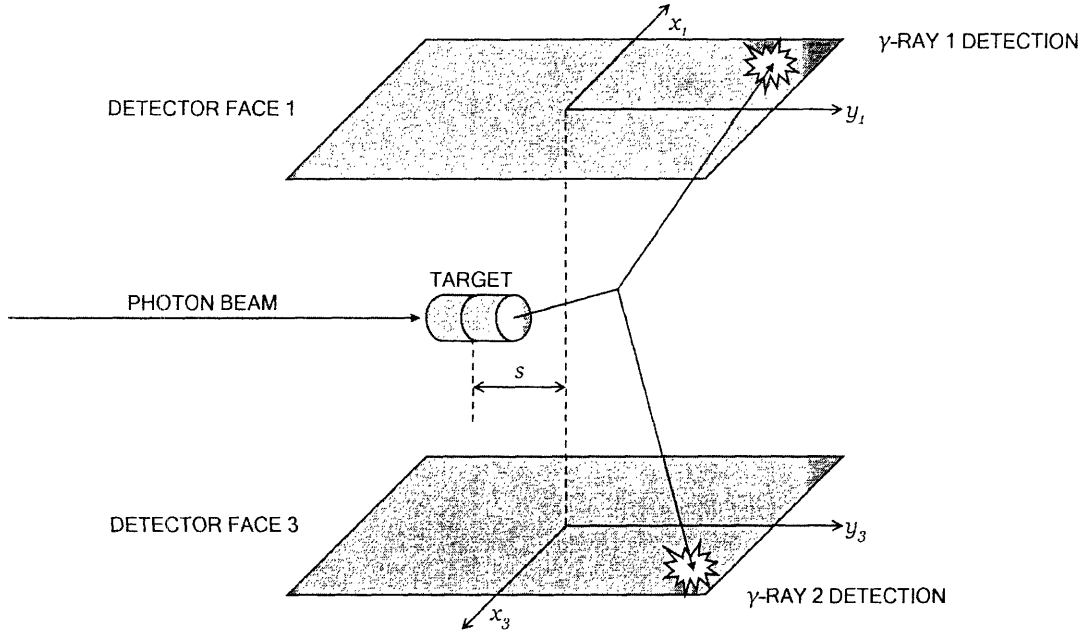


Figure 3-1: Coordinate systems on two opposing faces of the Crystal Box. Note that we shift the target by some distance s that maximizes the acceptance of the detector.

Face	Condition
$n = 0$	$\cos \phi > +1/\sqrt{2}$
$n = 1$	$\sin \phi > +1/\sqrt{2}$
$n = 2$	$\cos \phi < -1/\sqrt{2}$
$n = 3$	$\sin \phi < -1/\sqrt{2}$

Table 3.1: A systematic way of determining which face a γ -ray would hit if it lands on the detector. We do not need to consider the special case where a γ -ray hits the intersection of two faces since we are ignoring the outer edge crystals on each face.

Of course, we only have a limited resolution with our detector and cannot expect to measure these values exactly, so the second step is to blur these values to simulate the resolution of the actual detector. We need to add Gaussian errors to our coordinates that account for the limited position resolution provided by a crystal array, and a uniformly-distributed error only to the y -coordinate to take into consideration the fact that a pion may be produced anywhere along the length of the 10 cm target. We also need to add a resolution component to the energy. The following set of

parameters simulate what we will actually be able to reconstruct in our experiment:

$$x_{reconstructed} = x_{actual} + \varepsilon_x \quad (3.2a)$$

$$y_{reconstructed} = y_{actual} + \varepsilon_y + \varepsilon_s \quad (3.2b)$$

$$e_{reconstructed} = e_{actual} + \varepsilon_e \quad (3.2c)$$

Error	Source	Distribution
ε_x	Position resolution of crystal array	Gaussian with $\sigma = 0.8$ cm
ε_y	Position resolution of crystal array	Gaussian with $\sigma = 0.8$ cm
ε_e	Energy resolution of crystal array	Gaussian with $\sigma = 3\% \cdot e_{actual}$
ε_s	Finite length of target	Uniform on $[-5$ cm, 5 cm]

Table 3.2: Sources of error in the measurement of individual pion production events. The σ 's were calculated from the fwhm resolutions quoted in the previous chapter.

The third and last step is to reconstruct the cross section. From each individual scattering event we determine if the coordinates $\{x_{reconstructed}, y_{reconstructed}\}$ lie inside of the effective area of the detector. Since we are ignoring the outer edge crystals of the detector, the constraints for a γ -ray impact to be registered is that both $|x_{reconstructed}| \leq 25.4$ cm and $|y_{reconstructed}| \leq 28.6$ cm. If these conditions are met by both γ -rays, we proceed to calculate the momentum of each using its reconstructed point-of-impact coordinates and assuming the γ -ray is emitted from the center of the target (after all, the lifetime of the π^0 is extremely short!). Using conservation of momentum, we calculate the momentum of the pion, Lorentz-boost to the center of mass frame, and infer the CM angles at which the pion was created. By repeating the steps above for a large number of events we have created a procedure that implements the geometry and incorporates all physical properties of the Crystal Box detector relevant to the experiment.

3.2 Organization of tasks

We have chosen to divide the tasks of our simulations into separate scripts in order to facilitate development, keep the size of each script manageable, and possibly even reuse parts of the code to process data from the actual experiment.

The fraction of pions that we are able to detect in any direction (the *acceptance* of the detector) will vary significantly as a function of the angles of pion production due to the fact that we need *both* γ -rays to intercept the detector in order to detect a pion. Therefore we need to rescale the angular distribution of the pions that we actually detect in the experiment with the angular-dependent acceptance of the detector in order to reconstruct the cross section that we are measuring. Before beginning the simulation of the actual experiment, we use the script `pi0_photo_acc` to run a Monte Carlo simulation generating a large number of pion production events to be used in calculating the acceptance of the detector. This set of data differs from our simulation of the actual experiment in two fundamental ways: first, we produce the pions using a cross section with a uniform angular distribution in the CM frame. Second, we generate ten times more pions than we would expect during the actual experiment. These changes help improve the accuracy of our calculation of the acceptance independently of the data from the actual experiment. For each production event, the script `pi0hcsfull` the script determines if both γ -rays reach the detector. If this is true, it attempts to reconstruct the direction in which the pion was originally produced using only the position of impact of each γ -ray on the detector. Successful counts are binned in a histogram of 40×40 bins over ϕ^* and $\cos\theta^*$ and then divided by the total number of events generated in the direction of each bin, and this information is saved as the acceptance of the detector.

At this point we are ready to begin the simulation of the actual experiment! The script `pi0_photo_hp` runs a Monte Carlo simulation that generates a large number of pion production events using the cross section that we expect to observe in the actual experiment (equation 2.1). Simulation of this cross section requires us to choose a particular model to provide values for the CGLN amplitudes that we

Script	Task
pi0_photo_acc pi0hcsfull	Simulates production of pions using a uniform cross section, following by their decay into pairs of γ -rays. Simulates detection of γ -rays and reconstructs initial direction of pions. Calculates acceptance of detector.
pi0_photo_hp pi0hcthp	Simulates production of pions using the actual cross section, following by their decay into pairs of γ -rays. Simulates detection of γ -rays and reconstructs initial direction of pions. Calculates measured cross section.
filterscript	Prepares a data file by removing any empty bins due to a zero detector acceptance at the location of a bin.
fitdatascript	Fits multipoles using the reconstructed cross section.

Table 3.3: List of scripts and the task each performs in the simulation.

need in order to calculate the response functions defined in equations 2.2. We have chosen to use the DMT model calculations for the CGLN amplitudes. These calculations can be downloaded from the internet at <http://www.kph.uni-mainz.de/MAID/dmt/dmt2001.html>. Then (imitating the process carried by pi0hcsfull) the script pi0hcthp determines the fraction of pion production events that are measured by the detector in any given direction. After rescaling the counts by the acceptance of the detector calculated earlier, the script saves the simulated measurement of the cross section as a 40×40 histogram over ϕ^* and $\cos \theta^*$.

If the detector's acceptance is zero in any direction, rescaling by the acceptance fails to produce a sensible value for the cross section in that particular direction. For this reason we need to use the script filterscript to remove any empty bins from our data set and prevent any "zero error" data from wreaking havoc in our fitting script. Last, we use fitdatascript to fit the measured cross section to the functional form of equation 2.1 and extract values for the multipoles from our simulated observations.

Chapter 4

Results from the Simulation

4.1 Properties of the detectors

The first results to come out of the simulation are those that describe the properties of the Crystal Box detector itself starting with the detector's acceptance. One matter we have yet to address is finding the optimal target shift s from the center of the CB detector as illustrated in figure 3-1. We have the intuition that the shift must be in the opposite direction of the beam since the majority of the pions will scatter forward. We calculated the acceptance of the Crystal Box detector using values for s ranging from zero to 10 cm. The results are presented in figure 4-1 which shows that a value of $s = 5$ cm maximizes the mean acceptance, and we shall fix this value of s for the remainder of the simulation. At this value, the mean acceptance of the Crystal Box, 44.6%, is more than ten times larger than the mean acceptance of the NMS, 4.3%. Furthermore, as figures 4-2 through 4-4 illustrate, the acceptance of the Crystal Box is also far more uniform throughout the range of values of $\cos \theta^*$ and ϕ^* , giving the Crystal Box a much larger effective coverage area and making it better suited its task in this experiment.

Another interesting test of either detector is to calculate the accuracy with which it can reconstruct the fundamental kinematic properties of each pion photoproduction event. This accuracy will directly affect the resolution with which we can measure the cross section. For this purpose we have recorded the original angles of each pion

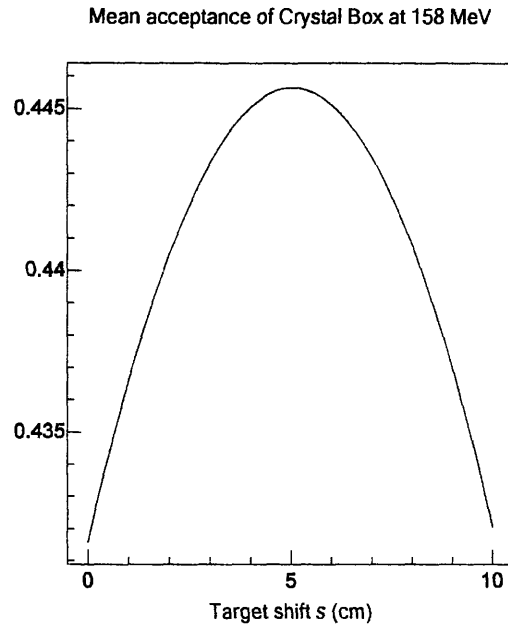


Figure 4-1: A plot of the mean acceptance of the Crystal Box as a function of target shift shows that the value $s = 5$ cm maximizes the mean acceptance of the detector.

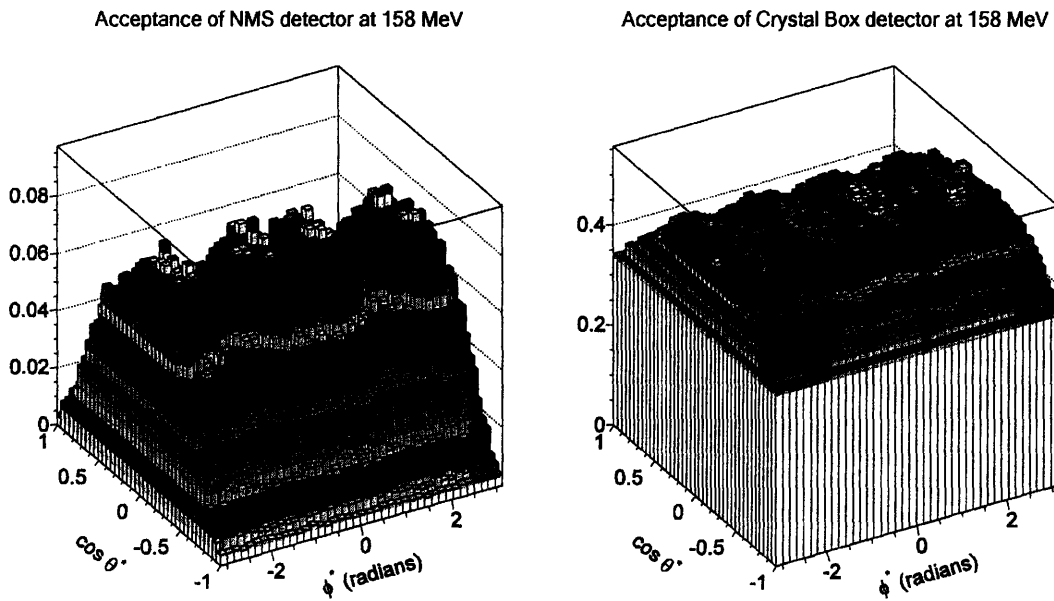


Figure 4-2: Acceptances of Crystal Box and NMS detectors. The acceptance of the Crystal Box is more uniform and much larger than the acceptance of the NMS.

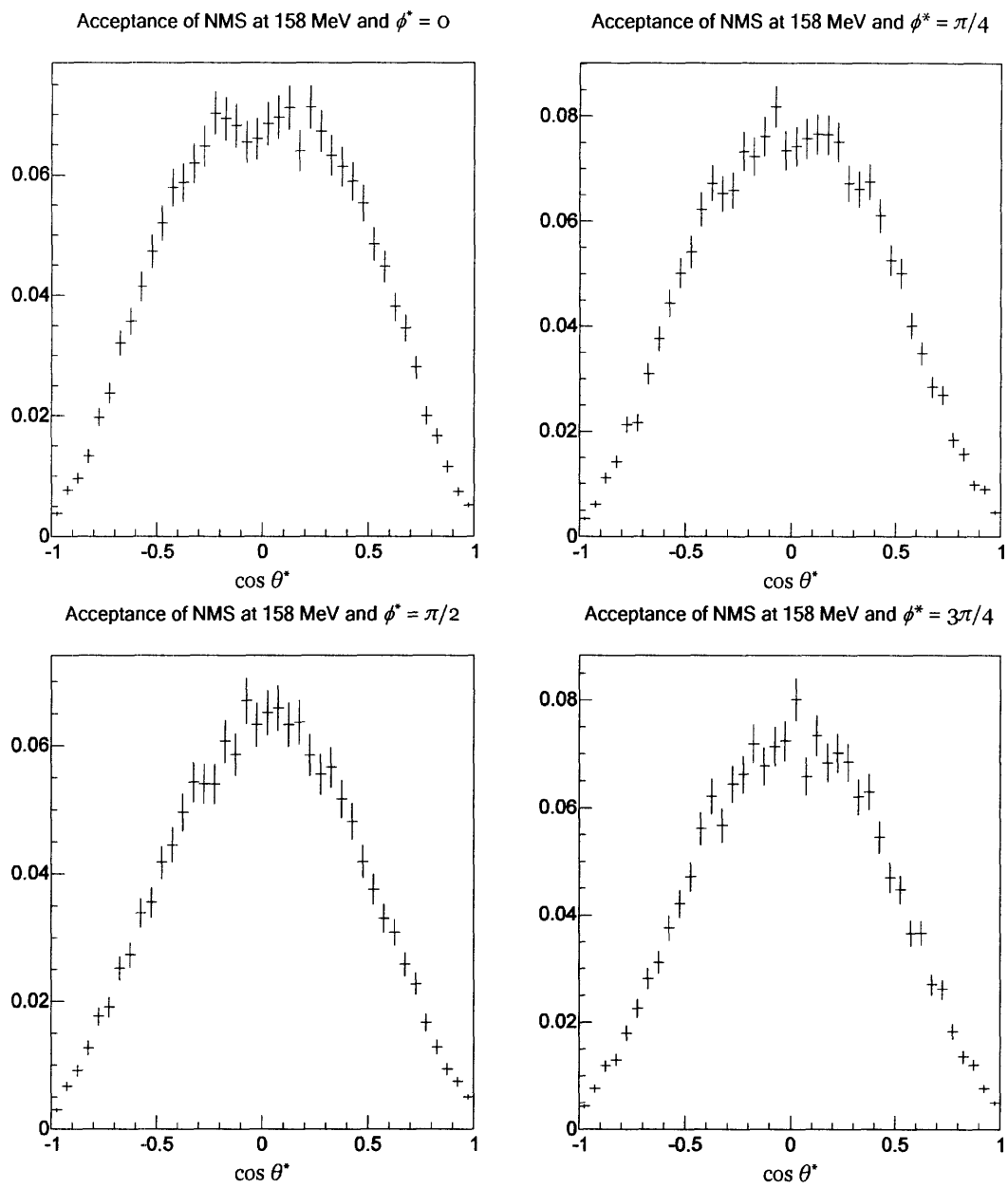


Figure 4-3: Slices of the acceptance of the NMS detector at fixed values of ϕ^* clearly illustrate the lack of uniformity in the acceptance of the NMS detector.

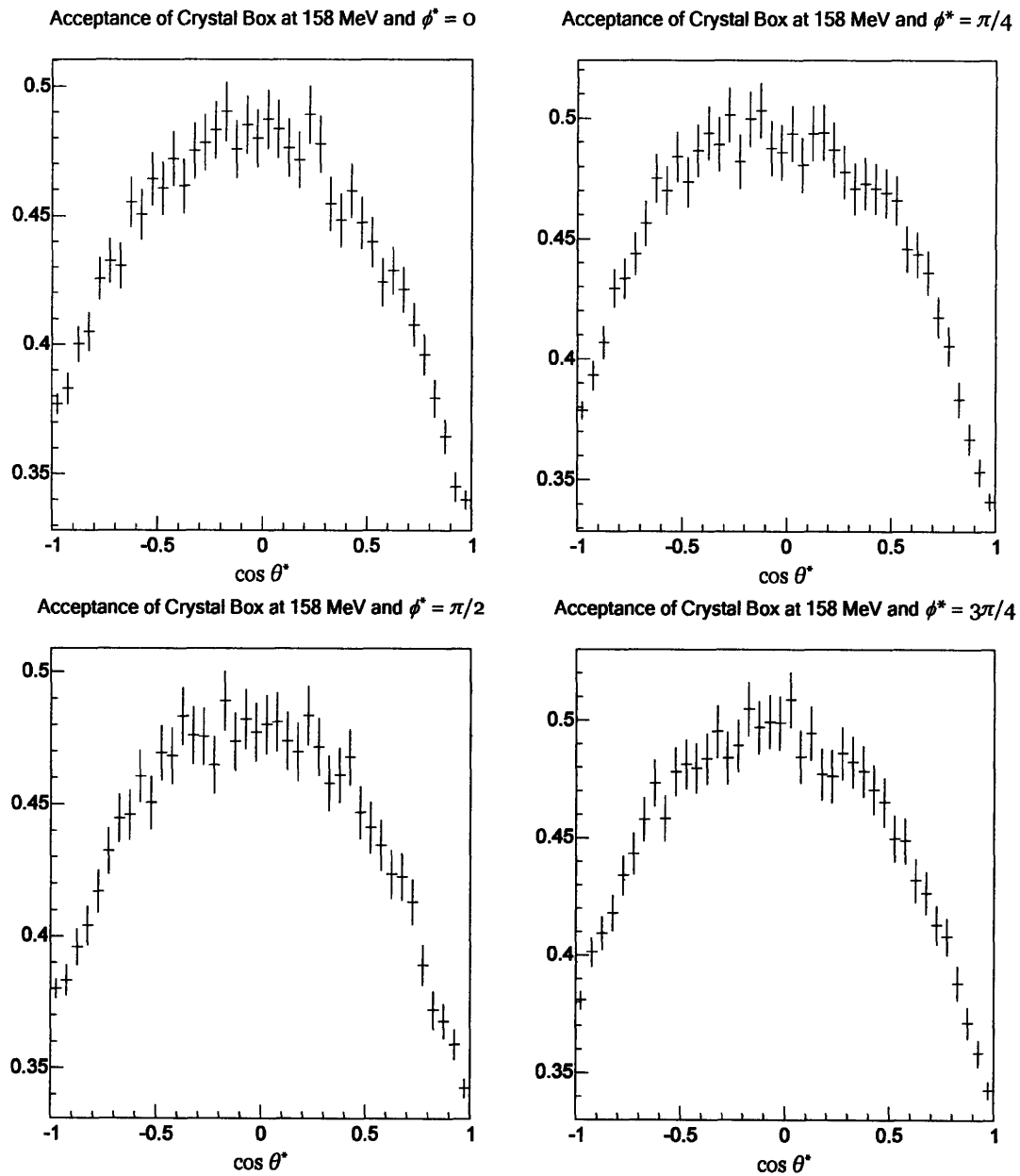


Figure 4-4: Slices of the acceptance of the Crystal Box at fixed values of ϕ^* . The range of values of the acceptance for the Crystal Box is far different from the NMS.

photoproduction event in the center of mass frame, ϕ^* and θ^* , the invariant mass of the pion m_π , and the combined energy e_{total} of both γ -rays. After reconstructing these quantities using the procedure described in chapter 3, we evaluate the quality of the reconstructed values by computing the quantities $\theta_{reconst}^* - \theta_{actual}^*$, $\phi_{reconst}^* - \phi_{actual}^*$, $m_{reconst}/m_{actual}$ and $e_{reconst}/e_{actual}$. We have binned this information in Figures 4-5 and 4-6, where we can observe that these quantities follow approximately Gaussian distributions. A quick fit to the data in each histogram reveals the standard deviation of these distributions which we interpret as the resolutions of the detectors:

Property	CB	NMS
Mean acceptance	44.6%	4.3%
Resolution of m_π	3.4%	3.8%
Resolution of e_{total}	2.4%	3.4%
Resolution of θ^*	5.0°	8.4°
Resolution of ϕ^*	0.4°	0.2°

Table 4.1: Acceptances and resolutions for both CB and NMS detectors. Resolutions for m_π and e_{total} are quoted as a percentage of the actual value of the each quantity.

The properties of the detectors summarized in table 4.1 will have a direct impact on the measurement of our data since these values describe not only how many events we will be able to measure on average, but also the resolution at which we can record the data. Most resolutions are significantly better with the Crystal Box as we would expect. However, the resolution for ϕ^* is surprisingly worse than if we were to use the NMS detector, though not by much. This effect is most likely attributable to the much larger solid angle we are able to capture with the Crystal Box together with its decreased resolution of γ -ray impact point measurements. However, the NMS already provides an excellent resolution of ϕ^* , so the lesser ϕ^* resolution of the Crystal Box is not a serious drawback and will be outweighed by better Crystal Box resolutions in the remaining observables.

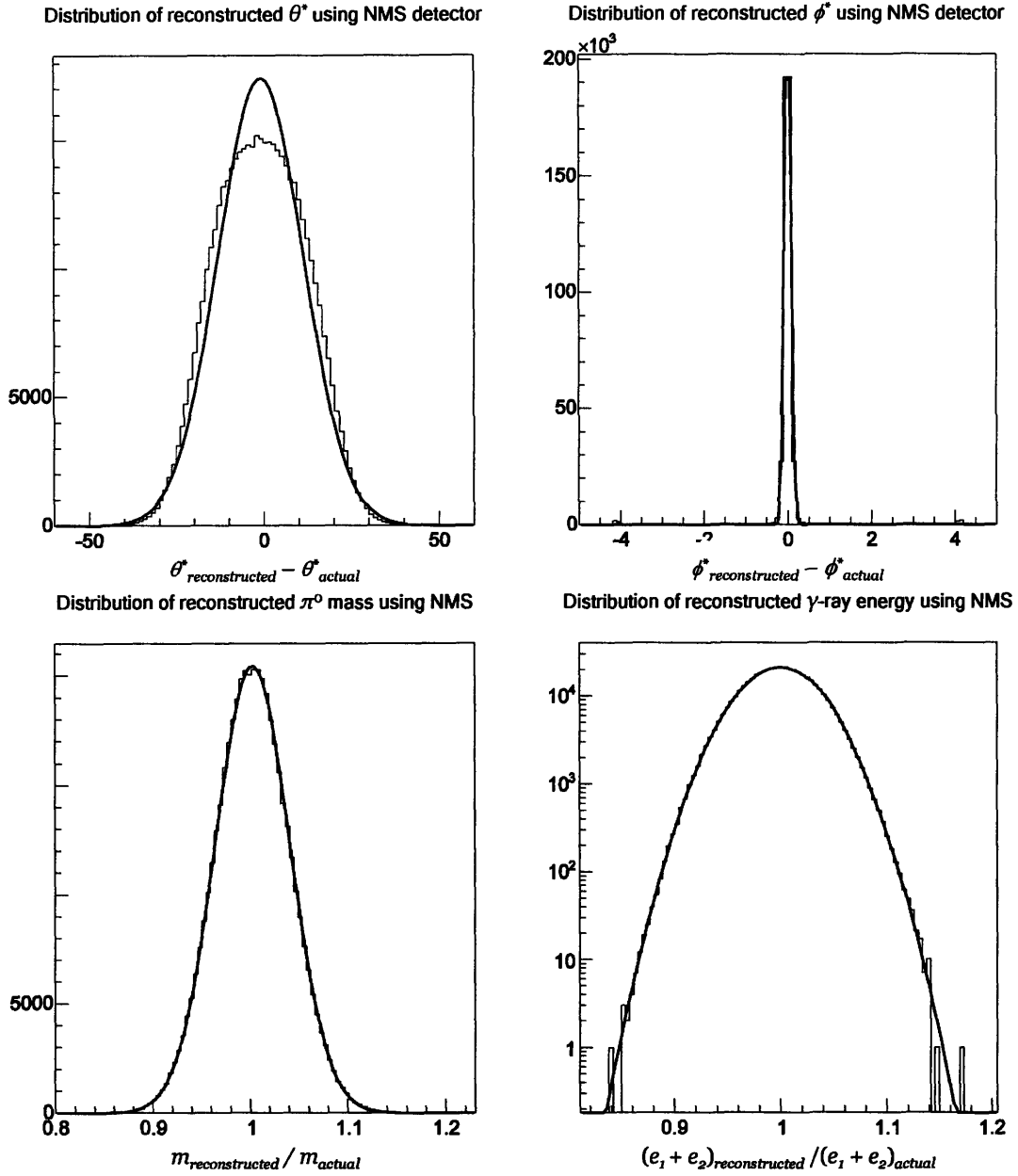


Figure 4-5: The distributions of errors in reconstructed ϕ^* , θ^* , m_π and e_{total} over all simulated events quantify the resolution at which the NMS can measure them.

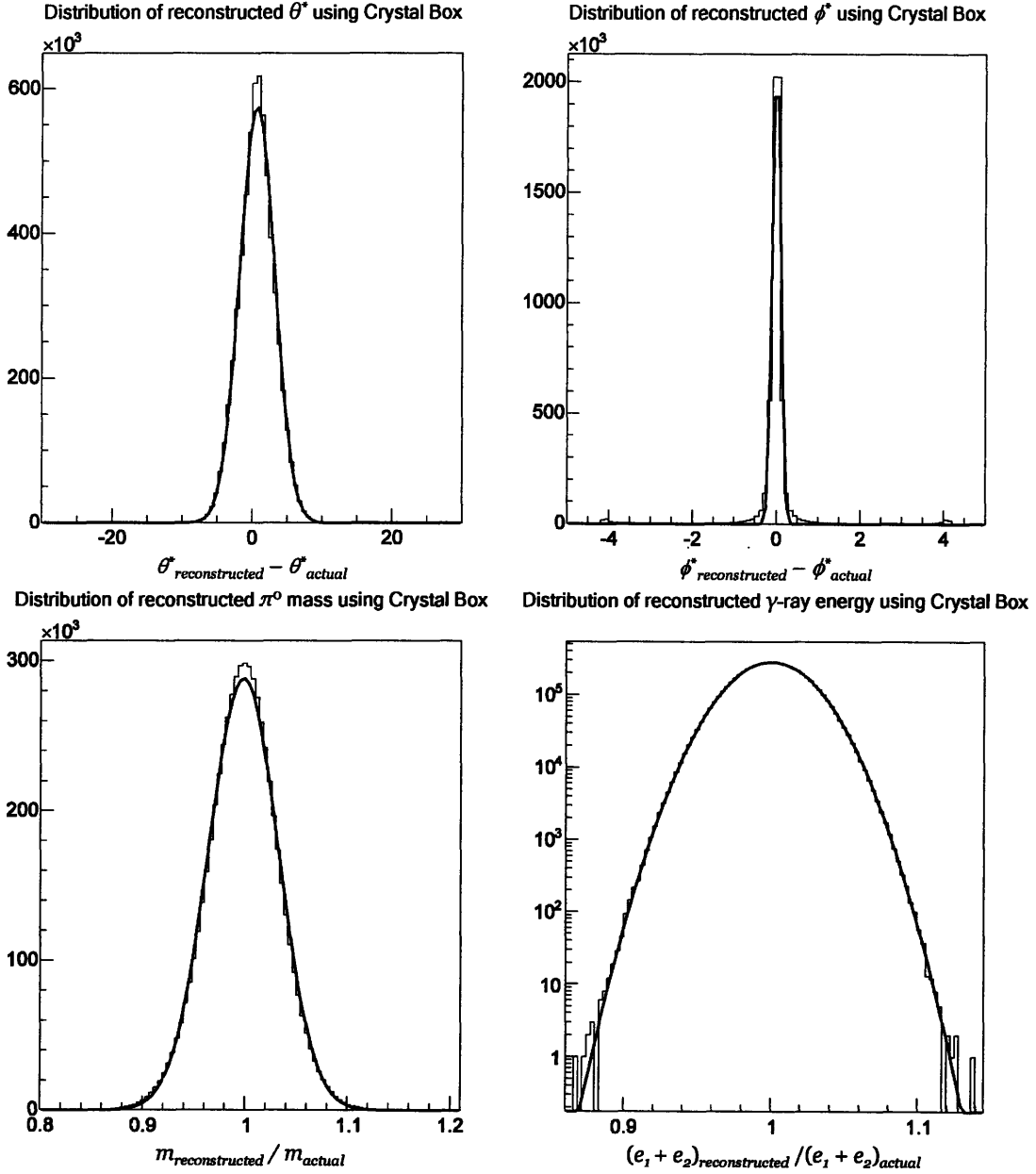


Figure 4-6: The distributions of errors in reconstructed ϕ^* , θ^* , m_π and e_{total} over all simulated events quantify the resolution at which the Crystal Box can measure them.

4.2 Fits to the simulation data

We are finally in a position to simulate the actual experiment! We use a beam of photons with a distribution of energies narrowly centered at 158 MeV with a spread of 2% fwhm. The beam is polarized normal to the floor, and each photon has equal probability of having either +1 or -1 helicity. We simulate a 200 hour experiment which, according to our calculation in chapter 2, works out to approximately 1.34 million pion photoproduction events. We set the polarization of the plastic scintillator target in the plane of the floor and perpendicular to the beam, though the simulation is designed to work with any desired combination of target and beam polarizations. Also, in order to preserve the additional information obtained from knowing the helicity of each incident photon, we group all photoproduction events by helicity producing +1 and -1 cross sections, but the fitting of all parameters is done using both cross sections simultaneously.

Figures 4-7 through 4-13 show slices of the cross sections we obtained by simulating detection using both Crystal Box and NMS detector. The most prominent aspect of the data is that we are able to measure the cross section over a much wider range of θ^* using the Crystal Box than what we are able to measure with the NMS. The multipole fits obtained from the simulated cross section are shown in tables 4.2 and 4.3. Note that not only are the errors obtained with the Crystal Box significantly smaller than those obtained with the NMS, but also that the Crystal Box fits are

Parameter	Fit	NMS	
		Statistical+Syst Error	Error %
$\Re[E_{0+}]$	0.839	0.192+0.001	22.9%
$\Im[E_{0+}]$	1.009	0.039+0.001	3.8%
E_{1+}	2.102	0.469+0.001	22.0%
M_{1+}	0.954	0.013+0.001	1.4%
M_{1-}	0.942	0.045+0.001	4.7%
		$(\chi^2_{\nu-1} = 1.17)$	

Table 4.2: Fits to simulation data using the NMS detector, with the parameters expressed as a multiple of the input value (such that 1.0 would be in perfect agreement). Note the bad fit for E_{1+} with the discrepancy being significantly larger than the error.

Parameter	Crystal Box		
	Fit	Statistical+Syst Error	Error %
$\Re[E_{0+}]$	0.991	0.049+0.001	5.0%
$\Im[E_{0+}]$	1.002	0.013+0.001	1.3%
E_{1+}	0.812	0.086+0.004	11.0%
M_{1+}	0.997	0.003+0.001	0.3%
M_{1-}	0.985	0.010+0.001	1.0%
		$(\chi^2_{\nu-1} = 1.25)$	

Table 4.3: Fits to simulation data using the Crystal Box, with the parameters expressed as a multiple of the input value (such that 1.0 would be in perfect agreement). Although the fit for E_{1+} is slightly off, the discrepancy is not too large as it is the case with the NMS. All fits are more accurate than the ones obtained using the NMS.

always in better agreement with the input values. In particular, while the fit of E_{1+} is in disagreement with the input value, the discrepancy is about an order of magnitude lower than when using the NMS detector, where the fit overestimates the value of E_{1+} by a factor of two. To identify the statistical errors of each fitted multipole, we ran a second simulation using the actual rather than reconstructed values of energy and impact points of the γ -rays. We then interpreted the errors in our fits to be entirely statistical, since our procedure leads to the exact angle determination for each pion production event.

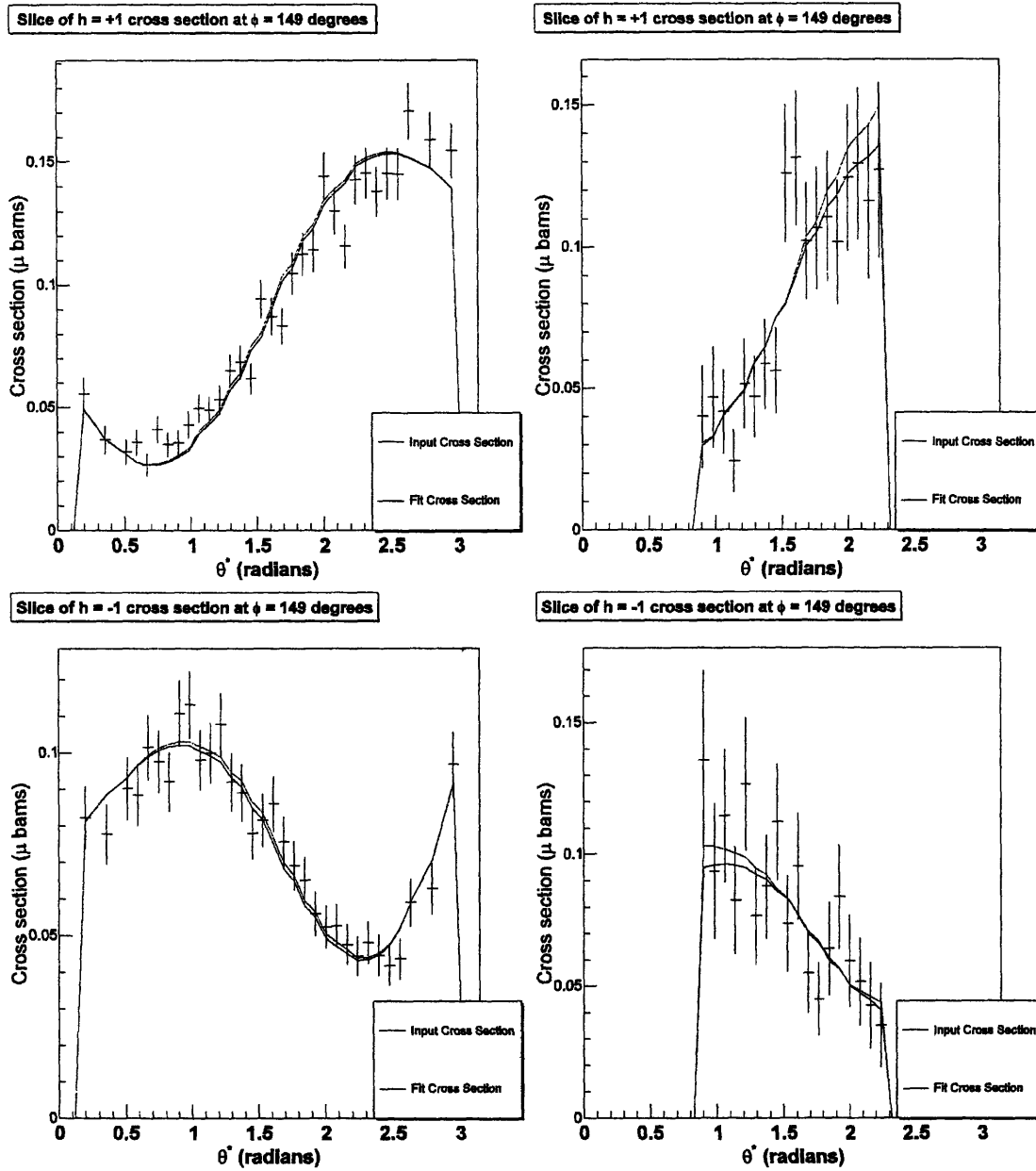


Figure 4-7: Simulated measurement of data using Crystal Box (left) and NMS (right) detectors. Each plot represents a slice of either $h = +1$ (top) or $h = -1$ (bottom) cross sections taken at $\phi = 149^\circ$.

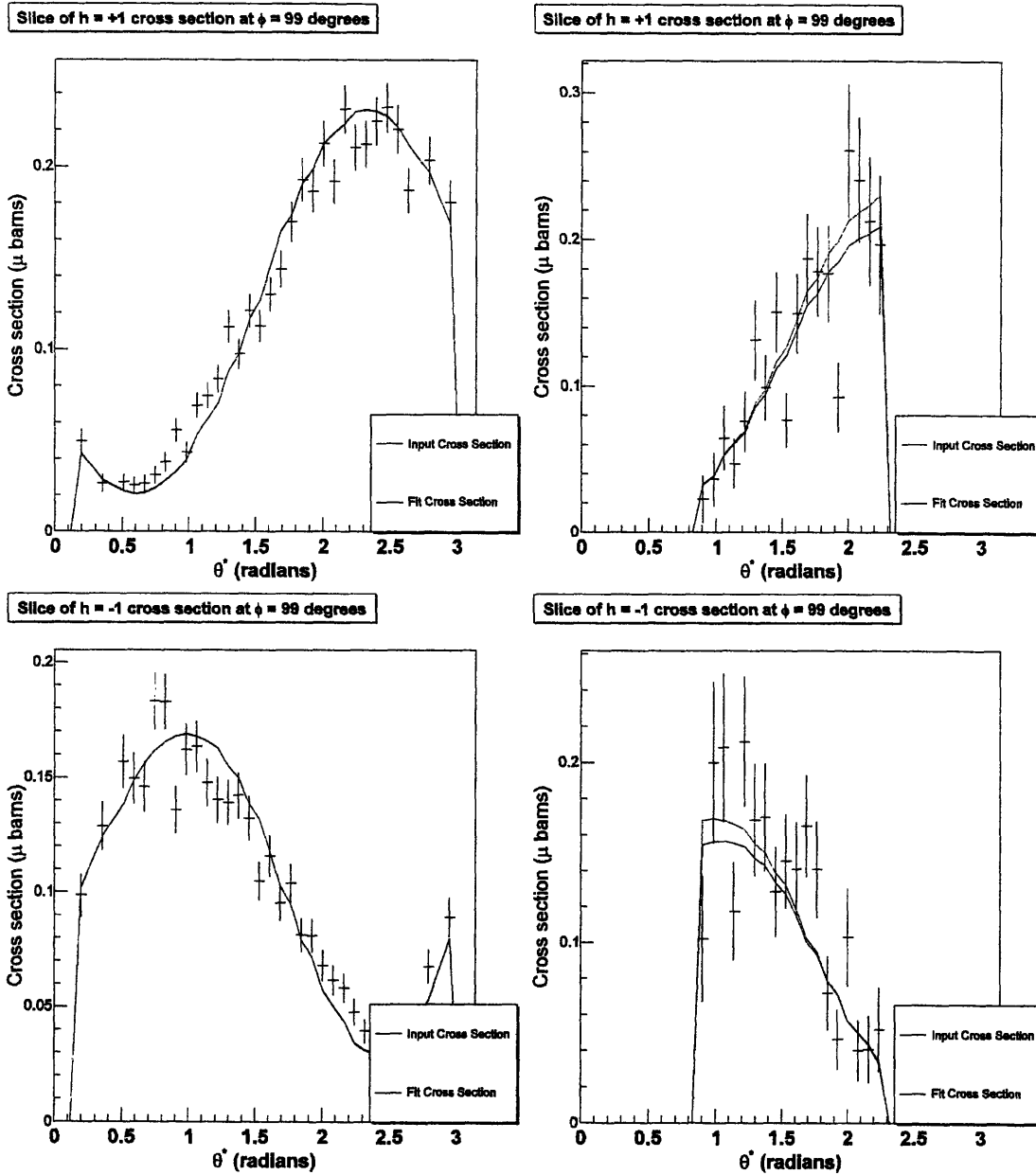


Figure 4-8: Slices of Crystal Box (left) and NMS (right) simulated data taken at $\phi = 99^\circ$. Note that the Crystal Box offers much broader coverage across θ^* resulting in a longer fitting region for the data.

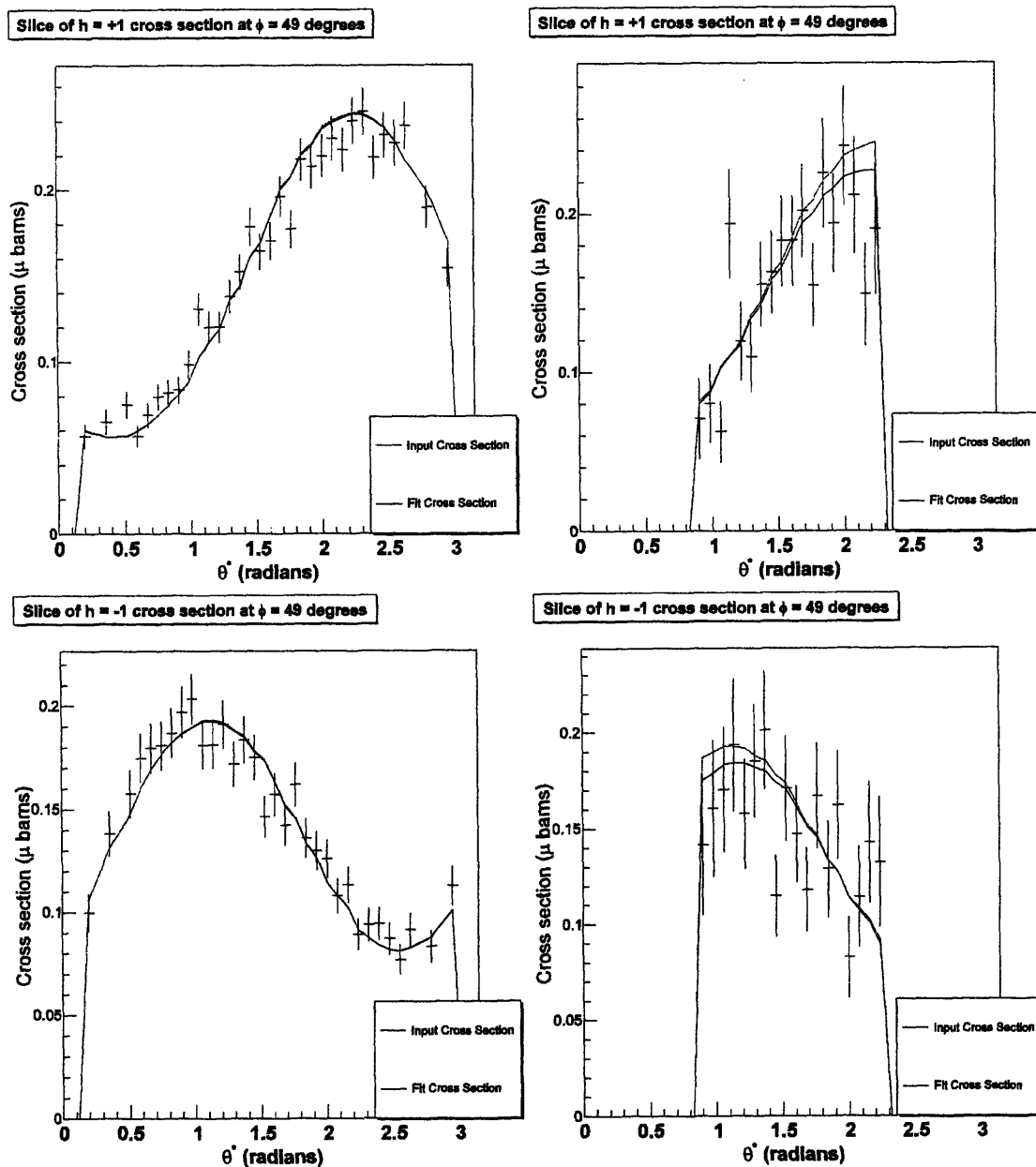


Figure 4-9: Slices of Crystal Box (left) and NMS (right) simulated data taken at $\phi = 49^\circ$. The fit of the data collected with the Crystal Box is significantly more accurate due to the improved statistics obtained with the use of this detector.

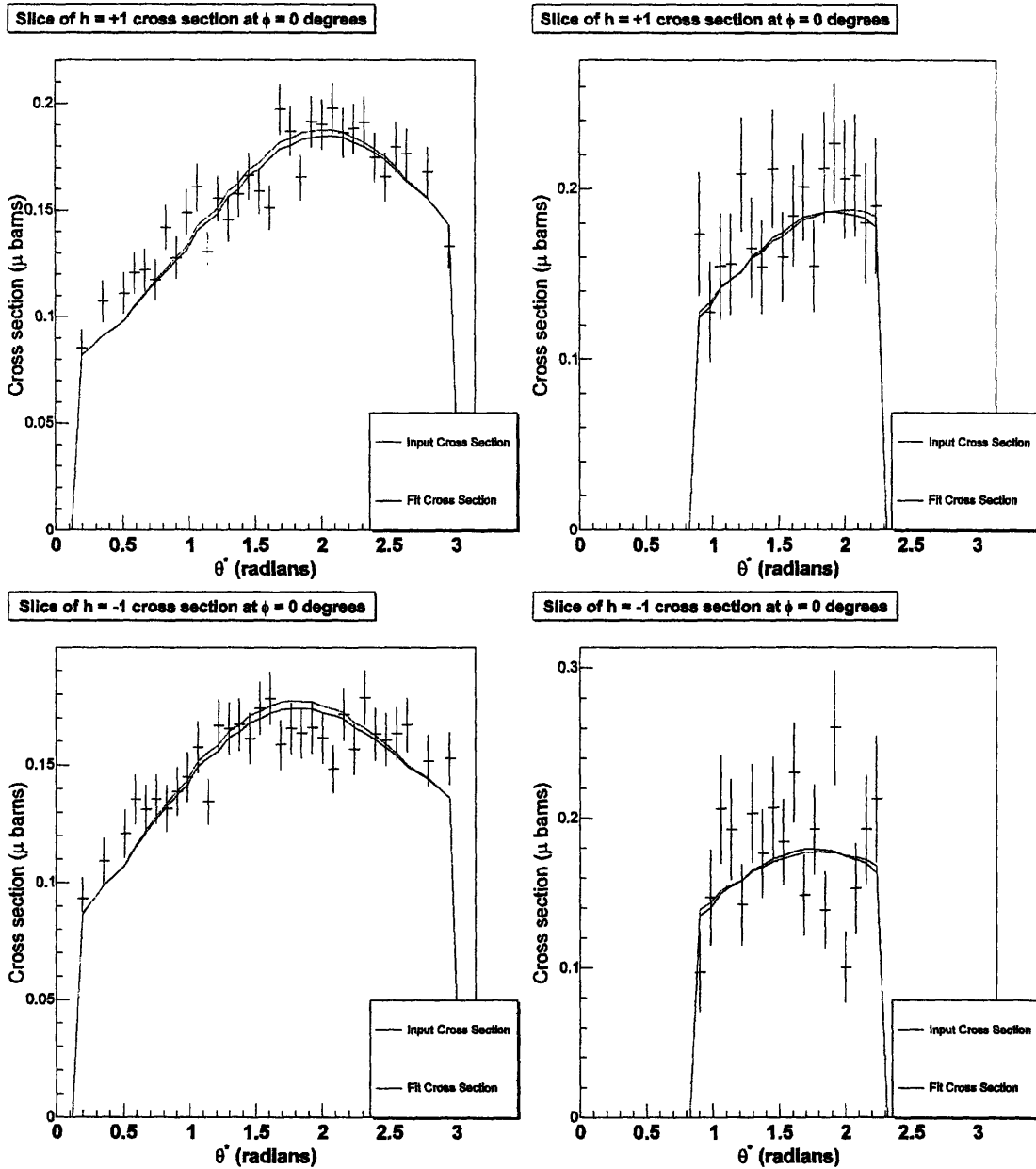


Figure 4-10: Simulated measurement of data using Crystal Box (left) and NMS (right) detectors. Each plot represents a slice of either $h = +1$ (top) or $h = -1$ (bottom) cross sections taken at $\phi = 0^\circ$.

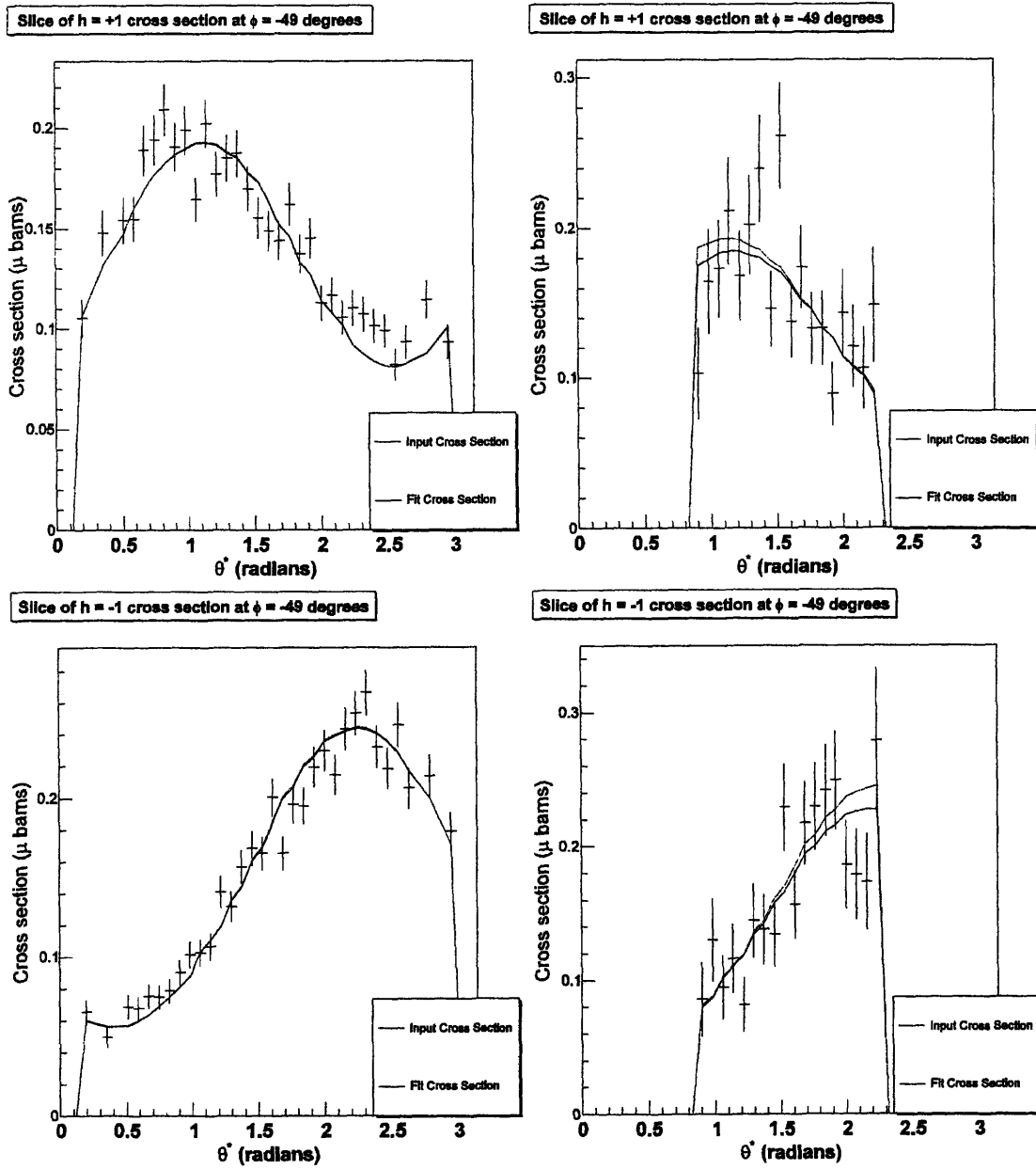


Figure 4-11: Slices of Crystal Box (left) and NMS (right) simulated data taken at $\phi = -49^\circ$. Note that the Crystal Box offers much broader coverage across θ^* resulting in a longer fitting region for the data.

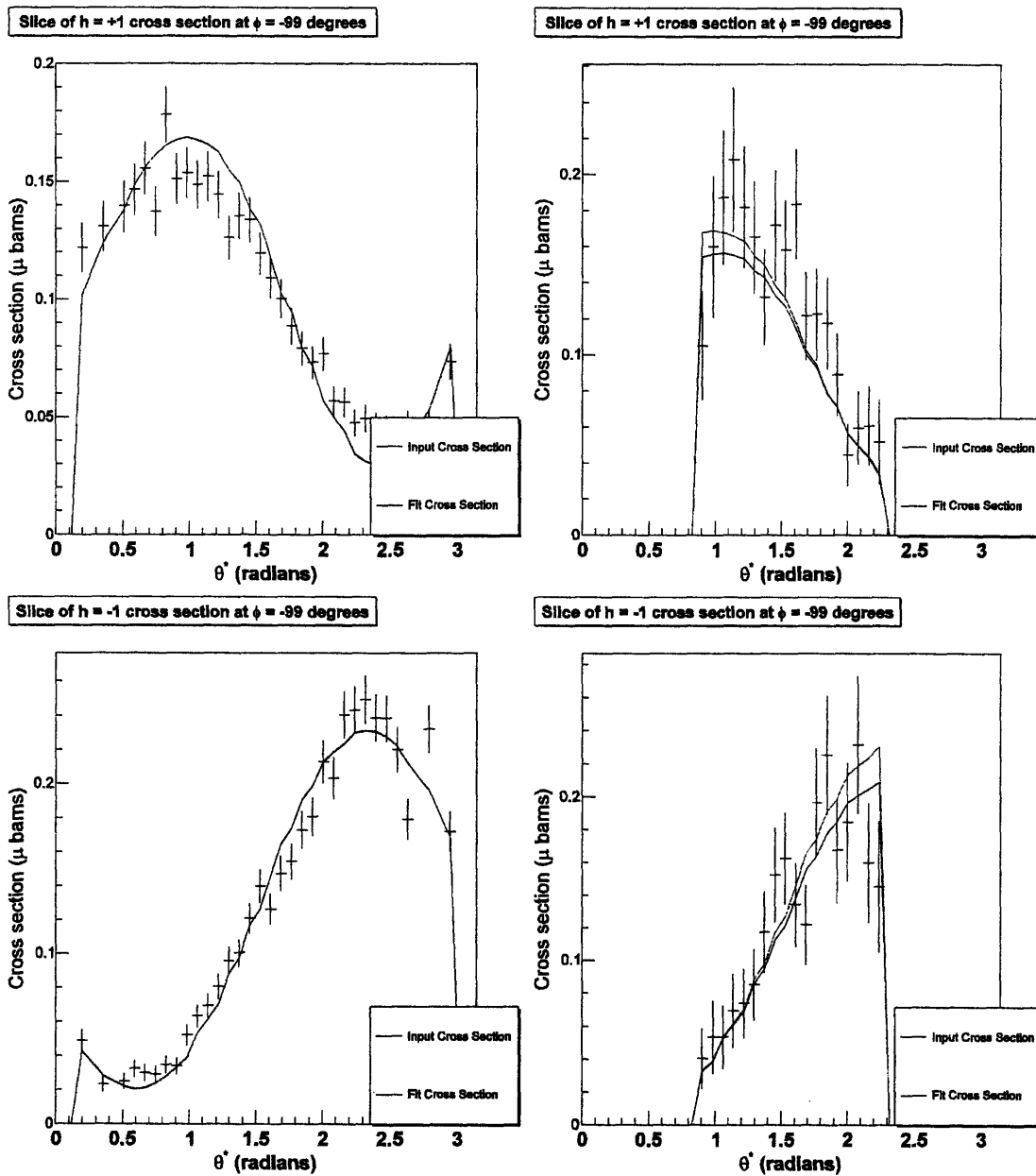


Figure 4-12: Slices of Crystal.Box (left) and NMS (right) simulated data taken at $\phi = -99^\circ$. The fit of the data collected with the Crystal Box is significantly more accurate due to the improved statistics obtained with the use of this detector.

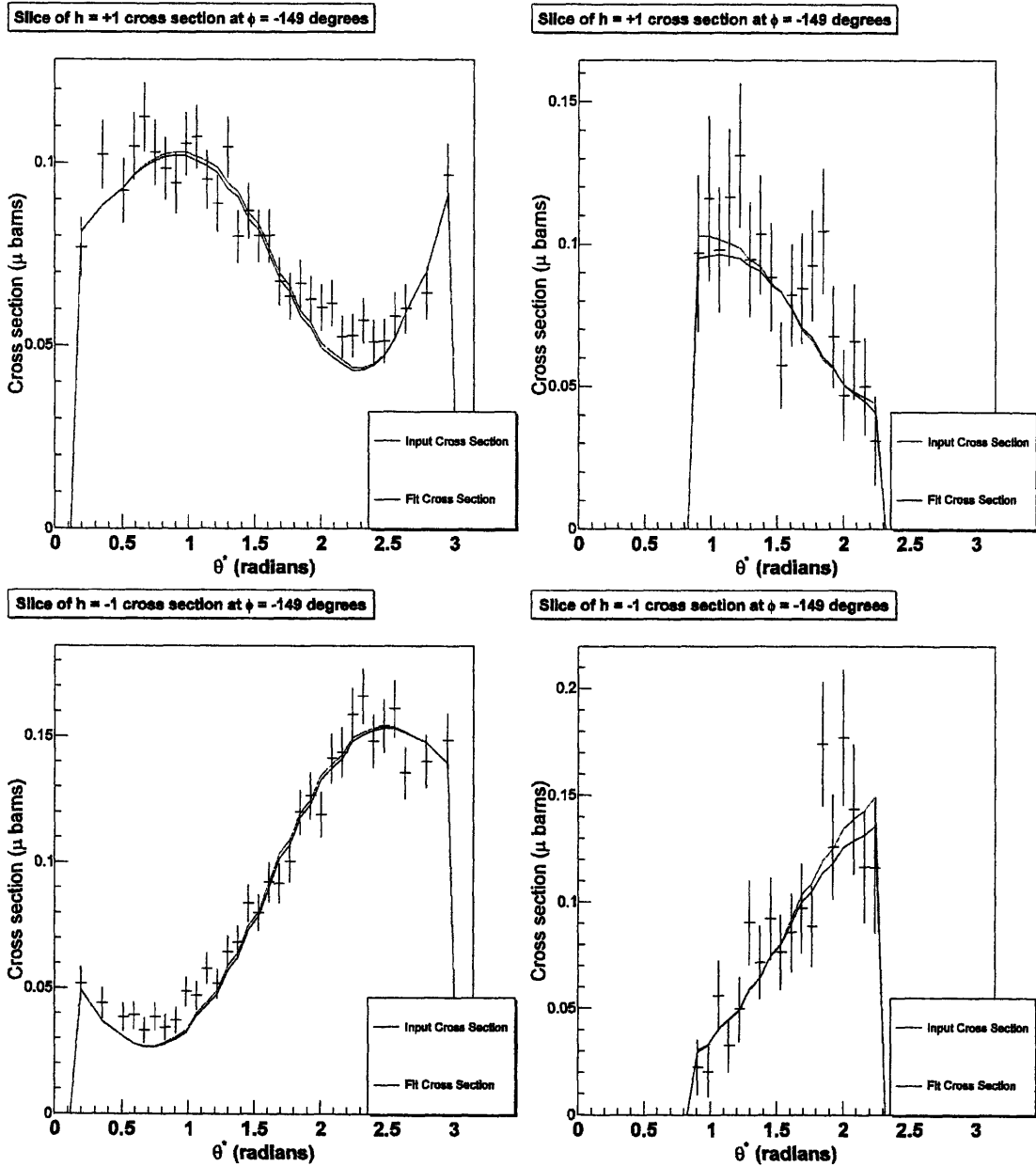


Figure 4-13: Simulated measurement of data using Crystal Box (left) and NMS (right) detectors. Each plot represents a slice of either $h = +1$ (top) or $h = -1$ (bottom) cross sections taken at $\phi = -149^\circ$.

Chapter 5

Conclusions

5.1 Performance of the detectors

We obtained substantially better fits (both in terms of precision and accuracy) for all multipoles by using the Crystal Box instead of the NMS detector in spite of the inferior resolution it provides in the measurement of γ -ray energy and point of impact. We credit this improvement to the much larger and uniform acceptance of the Crystal Box which has two direct effects on our data: first, we have a much wider range of θ^* where we can fit the cross section. Second, each cross section data point has much better statistics since we are able to detect more events under the same running time.

5.2 Limitations of the simulation

Although we have implemented the most relevant properties of the Crystal Box, there are still a few minor details we left out. For example, we accounted for the fact pions can emerge from anywhere along the length of the target, but ignored the consequences of using a target with finite thickness. This means there is also a distribution on the distance between where the pion is produced and the center of the photon beam, which we did not implement in our simulation. We are also assuming that the protons in our plastic scintillator target are completely at rest. In reality, the momentum of each proton has a distribution of non-zero width due to its finite

temperature. An improvement could be done by implementing these facts into our simulation. These and any other effects we may have ignored will work against our statistics, meaning that our estimates of the resolutions at which the experiment will be able to measure the multipoles are on the optimistic side.

We would also like to mention that we encountered a problem while attempting to make the simulation work with the target polarization parallel to the photon beam. This is a programming-related error that causes the simulation to try to fit the data collected with any detector to a functional form that does not resemble the data. We believe this is a software bug and not a feature of either detector because the error persists even if we simulate collection with an ideal (perfect coverage and resolution) detector, but the source of this bug is yet to be found.

Bibliography

- [1] H. Leutwyler. *Annals of Physics*, 235 165 (1994).
- [2] A.M. Bernstein et al. Photopion production measurements: tests of QCD chiral dynamics (internal proposed draft). 2005.
- [3] A. Schmidt et al. *Phys. Rev. Lett.*, 87, 232501 (2001).
- [4] Ethan Howe. Simulated pion photoproduction experiments. Undergraduate thesis, Massachusetts Institute of Technology, Department of Physics, May 2005.
- [5] G. Knöchlein, D. Drechsel, and L. Tiator. *Z. Phys*, A352 327 (1995).
- [6] W.R. Gibbs, Li Ali, and W.B. Kaufmann. *Phys. Rev. Lett.*, 74, 3740 (1995).
- [7] E. Matsinos. *Phys. Rev.*, C58, 3014 (1996).
- [8] D. Drechsel et al. *Nucl. Phys.*, A645 145 (1999). <http://www.kph.uni-mainz.de/MAID/>.
- [9] S.S. Kamalov, G.Y. Chen, S.N. Yang, D. Drechsel, and L.Tiator. *Phys. Lett.*, B522 27 (2001).
- [10] S.N. Yang, G.Y. Chen, S.S. Kamalov, D. Drechsel, and L. Tiator. *Nucl. Phys.*, A737 248 (2004). <http://www.kph.uni-mainz.de/MAID/dmt/dmt2001.html>.
- [11] S.L. Wilson et al. Design and performance of modularized NaI(Tl) detectors with rectangular crystal elements: an array of 49 and the Crystal Box. *Nuclear Instruments and Methods in Physics Research*, A264 263 (1988).